Asian Journal of Chemistry; Vol. 37, No. 8 (2025), 1885-1892

ASIAN JOURNAL OF CHEMISTRY

https://doi.org/10.14233/ajchem.2025.33992

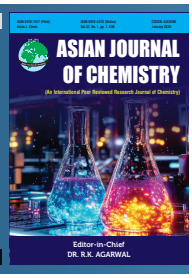

Synthesis and DFT Analysis of Thermoplastic Starch Bioplastics: A Sustainable Alternative for Green Packaging

DIVYANSHI MISHRA, INDU SAXENA*, ADITYA GUPTA and PREETI YADAV

Department of Chemistry, University of Lucknow, Lucknow-226007, India

*Corresponding author: E-mail: indu_lu@yahoo.com

Received: 5 May 2025; *Accepted*: 30 June 2025; *Published online*: 31 July 2025; AJC-22066

The growing environmental concerns about synthetic polymers have increased the need for biodegradable alternatives made from renewable resources. Starch, a naturally abundant and low-cost polysaccharide, appears to be a potential contender for long-term polymer applications. This work explores the structural and thermo-physical properties of thermoplastic starch (TPS) for use in the sustainable packaging. At 323.15 K, concentration-dependent behaviour was observed, with density increasing from 1026.5 to 1028.4 kg m^{-3} and viscosity increasing from 1.9855×10^{-3} to 2.1887×10^{-3} Ns m^{-2} as polymer concentration increased. Acoustic impedance increased proportionally (1606.47 to 1634.13 kg m^{-2} s^{-1}), but adiabatic compressibility fell from 3.9775×10^{-10} to 3.8511×10^{10} kg^{-1} ms^2, suggesting higher intermolecular interactions. DFT simulations showed that hydration improves the electrical stability of TPS by raising the HOMO-LUMO gap to 15.0763 eV, compared to 14.6969 eV for native starch. Thermodynamic study found that TPS had increased vibrational energy (281.045 kcal/mol) and entropy (187.904 cal/mol-K), confirming structural changes. Global reactivity descriptors indicated an improved chemical hardness (7.5382 eV) and decreased electrophilicity (0.0239 eV), confirmed improved material stability. Molecular docking revealed hydrogen bonding as the fundamental interaction mechanism (binding energy: -1.47 kcal/mol). These findings provide quantitative insights into TPS's adjustable features, emphasizing its promise as a sustainable alternative to traditional polymers.

Keywords: Potato starch, Biodegradable polymers, DFT, Hydrogen bonding interactions.

INTRODUCTION

The worldwide plastic pollution disaster has emerged as one of today's most severe environmental threats, with current production levels reaching 400 million metric tons per year and estimates of a triple by 2060 [1]. This unsustainable trajectory, combined with the disturbing reality that less than 10% of plastic trash is actually recycled, has created an urgent need for suitable biodegradable substitutes [2]. Among the numerous biopolymers under investigation, starch has emerged as the most promising due to its distinctive combination of absolute biodegradability, native abundance and cost effectiveness [3]. Starch, the second most abundant natural biopolymer after cellulose, has particular benefits for sustainable material development, with global output reaching 90 million tons per year from a variety of plant products including potato, wheat, potato and cassava [4].

Starch-based materials provide a variety of environmental benefits. Unlike conventional petroleum-based plastics, which can remain in the ecosystems for decades, starch biodegrades completely by microbial action, often mineralizing into carbon dioxide, water and biomass within months under the right climatic circumstances [5]. This essential distinction tackles the environmental permanence of synthetic polymers, one of their most significant drawbacks. Furthermore, a life cycle study of starch-based materials showed much lower energy requirements (25-55 MJ/kg) than petroleum-based plastics (75-100 MJ/kg), providing significant benefits in terms of carbon footprint and sustainability [6]. Starch manufacturing is carbon neutral and renewable, making it a major role in the transition to a cyclical bioeconomy.

The unusual molecular architecture of starch makes it a versatile platform for material development. Starch (Fig. 1a) has a semi-crystalline granular form and can be changed using various processing processes [7]. It is made up of two glucose polymers consisting of linear amylose (20-30%) and highly branched amylopectin (70-80%). The relative proportions of

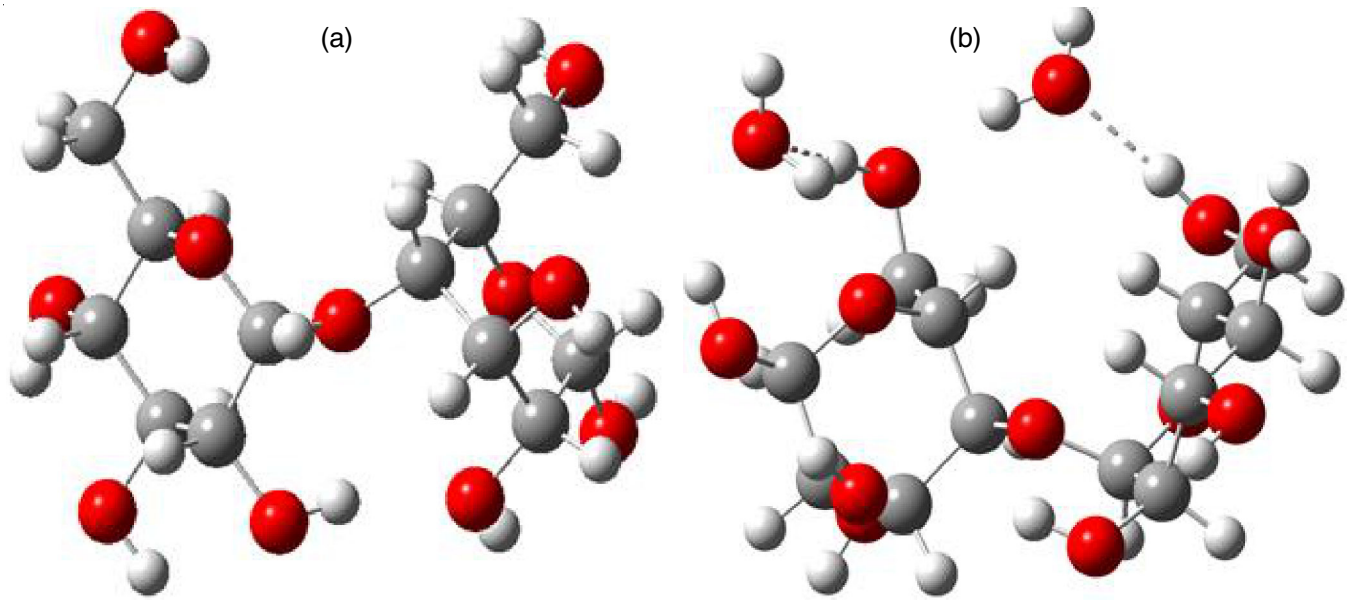

Fig. 1. Optimized structure of (a) starch (b) thermoplastic starch (TPS)

these components differ depending on the botanical source, allowing for the tweaking of material qualities. For example, high-amylose starches (50-80% amylose) produce stronger, more flexible films with better oxygen barrier qualities than regular or waxy starches [8]. This intrinsic diversity enables the development of starch-based materials with tailored characteristics for specific applications.

The invention of thermoplastic starch (TPS) (Fig. 1b) marks a significant advancement in starch-based material technologies. Heat and mechanical energy, in the presence of plasticizers, can change the native semi-crystalline starch structure into an amorphous thermoplastic material with much improved processability and mechanical qualities [9]. This transition involves breaking down hydrogen bonds between starch molecules and replacing them with hydrogen bonds with plasticizer molecules, resulting in a material that can be processed using traditional plastic manufacturing techniques like extrusion, injection molding and blow molding [10]. The glass transition temperature of TPS may be accurately adjusted by the kind and amount of plasticizer used, allowing for the manufacture of materials ranging from stiff plastics to flexible films [11].

Recent improvements in TPS technology have centered on overcoming its inherent limitations, specifically moisture sensitivity and mechanical property fluctuation. Nanocomposite techniques that include cellulose nanocrystals, nano-clays or other reinforcing agents have shown significant gains in mechanical strength and moisture resistance [12]. Chemical modification techniques such as esterification, etherification and crosslinking have been used to increase hydrophobicity and thermal stability [13]. These advancements have considerably increased the possible applications of starch-based materials, ranging from basic packaging films through more challenging uses such as agricultural mulch, disposable food service items as well as short-life consumer goods.

Advances in analytical techniques have greatly improved the characterization of starch-based products. Ultrasonic approaches have proven particularly useful for studying molecular interactions and structural features in polymer solutions, providing information about fundamental factors such adiabatic compressibility, acoustic impedance and relaxation events [14]. These measurements provide insight into the molecular interactions that control material behaviour, such as polymer-solvent interactions, aggregation processes and structural transformations [15]. Rheological characterization approaches have been essential in understanding and refining the processing behaviour of TPS, particularly its shear-thinning properties and thermal stability during processing [16].

In addition to these experimental approaches, the computational methods have developed as effective tools for understanding and forecasting the behaviour of starch-based systems. DFT simulations provide precise insights into electronic structure, molecular orbitals and reactivity descriptors, allowing for the prediction of chemical behaviour and interaction potentials [17]. Molecular dynamics simulations provide a dynamic perspective on molecular interactions, namely the behaviour of plasticizers within the starch matrix and the impact of hydration [18]. These computational approaches not only improve our fundamental understanding, but also speed up the development of new starch-based materials by eliminating the need for significant trial-and-error testing.

This study conducts a thorough evaluation of thermoplastic starch obtained from potato sources, using an integrated method that combines extensive experimental characterization and cutting-edge computational modeling. We are particularly interested in understanding the basic ties between molecular structure, processing factors and ultimate material qualities. Our experimental technique combines thorough ultrasonic characterization to probe molecular interactions with thermodynamic and mechanical property data. On the computational front, we use DFT calculations to investigate electrical structure and reactivity, as well as molecular docking studies to better understand specific interaction mechanisms. The combination

of these experimental and computational methodologies creates a strong framework for analyzing and enhancing starch-based products.

This study is important beyond academics since it provides the practical insights that could help with the commercialization of starch-based polymers. As the world transitions to more sustainable material systems, understanding the fundamental physics behind biodegradable alternatives becomes increasingly important. Our findings add to the expanding body of the knowledge that promotes the development of truly sustainable materials capable of serving modern society's diversified needs while addressing the critical environmental concerns posed by traditional plastics.

EXPERIMENTAL

Extraction of starch from potatoes: Potato starch was extracted in a specific manner to achieve optimal yield and purity. Potatoes were first rinsed with warm water to eliminate surface debris before being peeled. Potatoes had been peeled and mashed. To separate the juice from the mashed potatoes, a laboratory-grade juicer was used. The resulting slurry, which contained starch granules, broken cell walls and other soluble components such as proteins, amino acids, carbohydrates and salts, was passed through muslin cloth. To extract as much starch as possible, more water was applied to the residue on the fabric. The filtered liquid was collected in a glass beaker and sieved through two fine mesh sieves with pore diameters of 200 and 100 µm. Following sieving, the filtrate was allowed to settle for 4 h, allowing starch particles to settle. The sedimented starch was isolated from the supernatant and resuspended in water. This washing operation was carried out five times to ensure the complete cleaning. Finally, the purified starch was dried in an oven at 40 ºC to produce the final product.

Preparation of bioplastic film: Initially, a preset amount of potato starch was dissolved in distilled water in a 250 mL glass beaker using continuous magnetic stirring to guarantee uniform dispersion. Glycerine was added to the starch-water solution. To avoid the lump formation, the mixture was heated under regulated conditions on a hot plate with constant agitation. As the temperature increased, the starch solution gelatinized, changing from a murky suspension to a thick, translucent gel. The resulting polymeric solution was then cast onto a Teflon plate, forming a thin, homogeneous coating. The cast film was dried in a controlled oven setting to allow the solvent to evaporate and the film to solidify. For concentration-dependent experiments, a primary stock solution (0.002 M) was generated first, followed by the addition of potato starch in stages to achieve higher concentrations (0.004 M and 0.006 M). Prior to casting, each formulation was homogenized with the heating mantle to produce a clean and transparent polymeric solution.

Physical parameters

Ultrasonic sound velocity measurement: Using a single crystal ultrasonic interferometer with a 2 MHz frequency (Model-83S), provided by Mittal enterprises, New Delhi, India that has an accuracy of 0.4 m s^{-1} at 25 ºC, ultrasonic velocity (U) was recorded at 323.15 K [19], using eqn. 1:

$$U = n \times \lambda \quad (1)$$

Density measurement: By using a magnetic float densitometer at various temperatures, the densities of these solutions were calculated. The densities of these polymeric solutions were computed using eqn. 2:

$$\text{Density (d)} = \frac{W + w + f \times I}{V + w/d_{pt}} \quad (2)$$

where W = weight of float, w = weight put on the float, f = weight equivalent current (g/amp), V = volume of float, d_{pt} = density of platinum, I = current passing in the circuit [20].

Viscosity measurement: Viscosity (η) measurements were made using Ostwald's viscometer. The viscometer was placed in a water bath after being filled with the reference liquid (distilled water) [21]. To calculate the viscosity (η) of unknown polymeric solutions using the time required for the distilled water and mixture, eqn. 3 was used:

$$\frac{\eta_s}{\eta_w} = \frac{\rho_s}{\rho_w} \times \frac{t_s}{t_w} \quad (3)$$

where η_w, ρ_w and t_w are the viscosity (Poise), density (g/cm^3) and time flow of water (s), respectively and η_s, ρ_s and t_s are the viscosity (Poise), density (g/cm^3) and time flow (s) of unknown experimental solution, respectively.

Computational studies

DFT studies: Density functional theory (DFT) computations were used to analyze the structural, thermodynamic and electrical aspects of the systems being studied [22]. All DFT computations were performed using the Gaussian 09 software package, which included the B3LYP hybrid functional because of its known accuracy in predicting molecular characteristics and thermodynamic parameters. For geometry optimizations and frequency computations, the 6-311++G(d,p) basis set was used, which incorporates diffuse and polarization functions to optimize electron distribution and molecule interactions [23]. In present work, we have examined several aspects pertaining to the molecules' total chemical reactivity. The chemical reactivity of a molecule or complex can generally be expressed using a range of reactivity metrics, including chemical potential, ionization potential, electron affinity, chemical hardness, chemical softness, electrophilicity index, nucleophilic index and so forth [24]. The calculated values of these parameters can be examined using the Frontier Molecular Orbital (FMO) theory [25].

In conclusion, the FMO theory asserts that the electron density of the molecular orbitals determines how molecules interact with one another during a reaction and the possibility of associated structural or functional changes. In other words, the global reactivity indices, also known as the overall chemical reactivity, can be obtained by computing the quantum parameters after estimating the molecule's excitation properties using FMO theory. Furthermore, it is reasonable to expect that a molecule with a lower energy difference between the HOMO and LUMO orbitals will be more reactive to sensitive transformations. On the other hand, a large energy difference between the HOMO and LUMO suggests that the molecule is stable

and may not be involved in chemical reactions or have much reactivity. Collectively, the global reactivity indices can reveal information about the reaction's structural characteristics, chemical reactivity and possible bonding locations.

Molecular docking: The AutoDock 4.2.6 program was used in an *in silico* docking study to estimate the binding mode interactions between compounds. This program analyzes binding energy quickly using a semi-empirical free energy force field, the Lamarckian genetic algorithm and a grid-based approach. To produce stable conformations, the molecular structures of water and starch were first sketched using ChemDraw (Perkin-Elmer, USA) and then transformed into 3D geometries using Chem3D. Energy minimization was then performed. AutoDock Tools, a feature of AutoDock 4.2.6, was used to create the optimal structures for docking and save them in.pdb format [26]. After assigning Gasteiger charges and adding polar hydrogens, the structures were saved in the .pdbqt format. Both structures were regarded as stiff during docking, with water serving as the ligand and starch as the macromolecule in this investigation. The Lamarckian Genetic Algorithm (LGA) was used for docking with the conventional parameters after a grid box covering the full starch structure was created. After the docking simulations were finished, interaction profiles were examined and binding postures were graded according to binding energy [27].

RESULTS AND DISCUSSION

Acoustic studies: Studies on the aqueous solution of thermoplastic starch (TPS), the thermo-physical characteristics and acoustic aspects at various concentrations (0.002, 0.004 and 0.006 M) were conducted at 323.15 K. The calculated acoustic features, including adiabatic compressibility (β_{ad}), acoustic impedance (z), relaxation time (τ), free path length (L_f) and other parameters, are described in Table-1. It was revealed that when the concentration of the polymer solution increases, more polymer chains are added to the solution, increasing density as more solutes are added. Only the presence of a significantly higher temperature, at which density rapidly lowers, could explain this trend in the density of solution [28].

In present study, the viscosity (η) grows in proportion to the molar concentration. The viscosity of a liquid measures how difficult it is for the fluid to flow; as the force of resistance increases, so does the viscosity value. The amount of molecules in a solution also influences its viscosity; the more molecules there are, the less viscous the fluid. Every time a change happens, it could be due to significant forces formed between the layers of the solution and the polymer [19]. It was found that the ultrasonic velocity (u) of a polymer solution often increases with concentration, indicating a strong solute-solvent interaction.

The adiabatic compressibility (β_{ad}) decreases concentration dependently (Fig. 2a), indicating increased molecular packing and intermolecular interactions despite minimal ionic repulsion. This pattern is consistent with the inverse association between ultrasonic velocity and β_{ad}, supporting Eyring and Kincaid's assertion that higher sound velocity indicates stronger solute-solvent interactions. The stiffness of polymer chains rises with larger polymer concentrations due to restricted rotational freedom of monomer units, which amplifies the frictional forces and limits segmental motion. This trend is similar across all examined systems, demonstrating the importance of intermolecular interactions in determining solution dynamics.

Acoustic impedance (z), a measure of medium resistance determined by internal pressure and elasticity, progressively increases with concentration (Fig. 2b), indicating increased intermolecular contacts between polymeric and starch molecules [29,30]. The lack of solute-solute complexation, combined with the dominance of H-bonding (facilitated by -OH groups), reinforces the preponderance of solute-solvent and solvent-solvent interactions.

The relaxation period (τ) increases with concentration (Fig. 2c), indicating that viscous forces dominate the relaxation process. This elongation is caused by chemical interactions between starch and water molecules, which reduce segmental mobility and increase free energy. The observed ultrasonic velocity trend cannot be attributed exclusively to relaxation dynamics, showing that molecule cooperativity, hydrogen bonding and structural rearrangements all contribute to the thermophysical properties of system.

The intermolecular free length (L_f) decreases with increasing concentration (Fig. 2d), reflecting the β_{ad} behaviour. This reduction emphasizes strong intermolecular interactions, notably H-bonding, at higher concentrations. At dilute concentrations, repulsive forces predominate, indicating weaker interactions.

Molecular docking: The molecular docking investigation of water with starch was completed successfully using AutoDock 4.2.6. The binding energy (BE) for the optimal docked conformation was determined to be -1.47 kcal/mol. The docking study revealed the presence of two hydrogen bonds between the water molecule and the hydroxyl groups of the starch monomers as depicted in Fig. 3 [31].

It is critical to observe that the current docking work used a highly simplified model system, with only a small fraction of the complete starch polymer and a single water molecule. In genuine biological and material systems, starch is a huge

TABLE-1
VALUES OF VISCOSITY, DENSITY, ULTRASONIC VELOCITY, ADIABATIC COMPRESSIBILITY (β_{ad}), ACOUSTIC IMPEDANCE (z), RELAXATION TIME (τ) AND FREE PATH LENGTH (L_f) FOR THE POLYMERIC SOLUTION AT 323.15 K

Conc. (M)	ρ (Kg m^{-3})	$\eta \times 10^{-3}$ (NSm^{-2})	U (ms^{-1})	$\beta_{ad} \times 10^{-10}$ (kg^{-1} ms^2)	$z \times 10^3$ (kg m^{-2} s^{-1})	$\tau \times 10^{-13}$ (s)	$L_f \times 10^{-11}$ (m)
0.002	1026.5	1.9855	1565	3.9775	1606.47	10.5034	4.7837
0.004	1027.8	2.0699	1576	3.9172	1619.81	10.7839	4.7473
0.006	1028.4	2.1887	1589	3.8511	1634.13	11.2104	4.7071

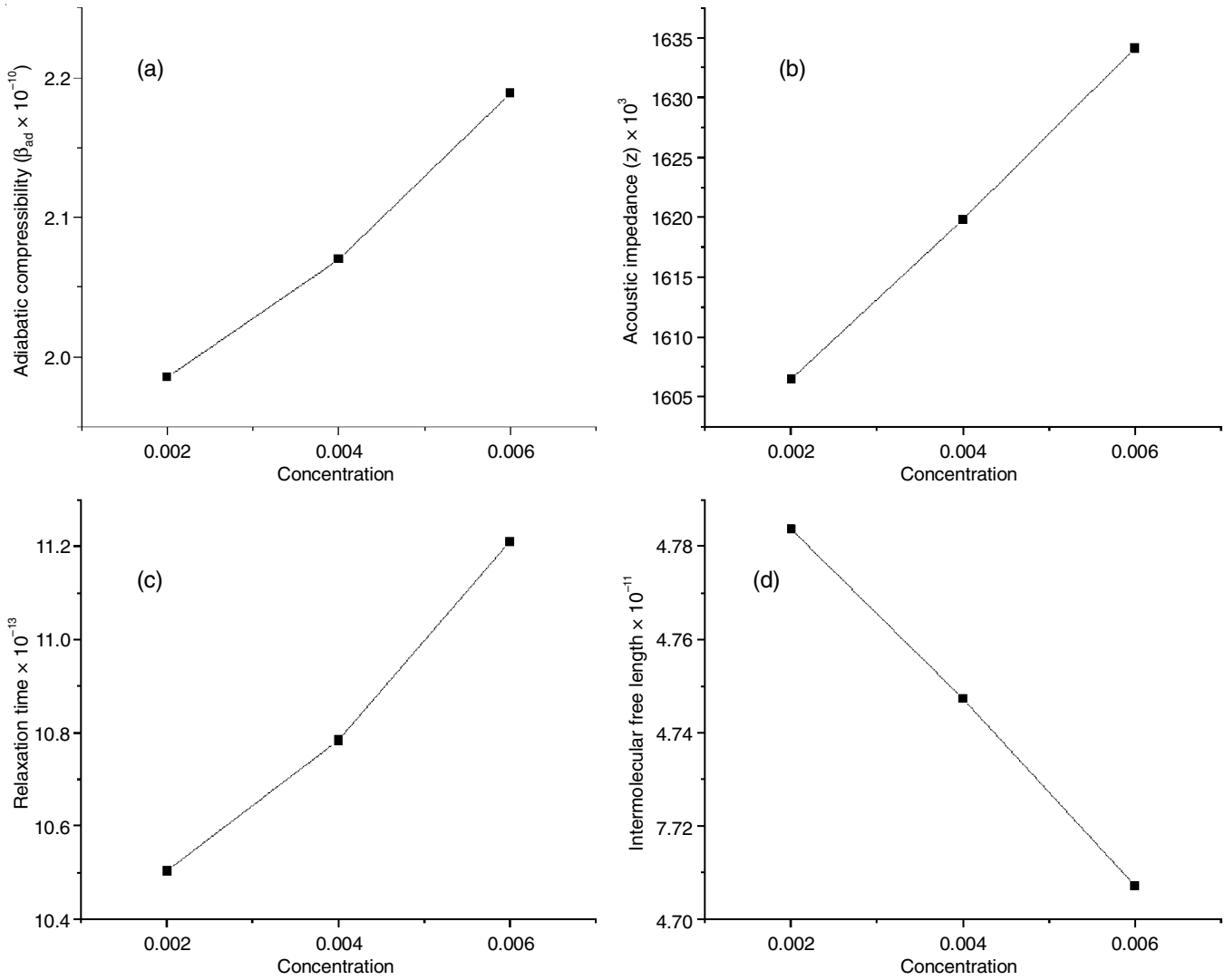

Fig. 2. (a) Variation of adiabatic compressibility (β_{ad}) (× 10^{-10} kg^{-1} ms^2), (b) acoustic impedance (z) (× 10^3 kg m^{-2} s^{-1}), (c) relaxation time (τ) (× 10^{-13} sec) and (d) intermolecular free length (L_f) (× 10^{-11} m) with polymeric solution concentration

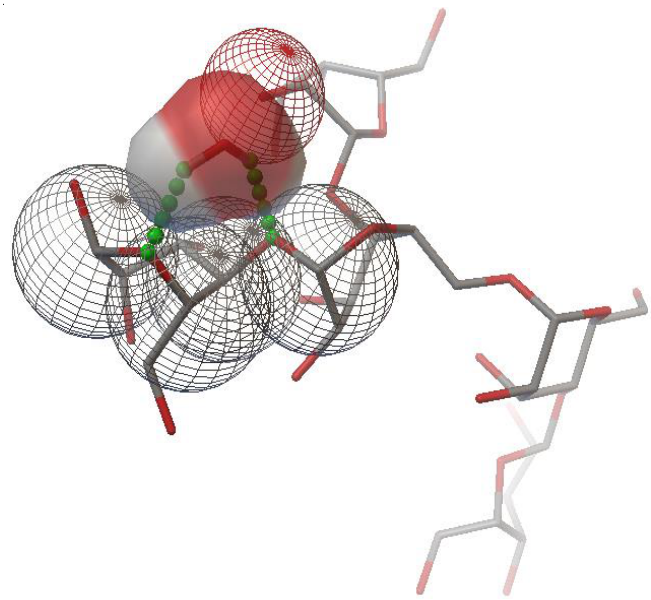

Fig. 3. Hydrogen bond interactions between starch and water ligand

polysaccharide comprising hundreds to thousands of glucose monomers that interact with millions of water molecules. As a result, the overall binding energy in a genuine hydrated starch system would be the sum of several individual interactions, such as many hydrogen bonds and van der Waals forces. While the binding energy produced for a single water-starch interaction is minimal, the cumulative effect of large, dynamic bonding networks would greatly affect the macroscopic features of starch, such as its swelling, hydration and gelatinization behaviour [32].

FMO analysis: Frontier molecular orbitals (FMOs) of starch and its hydrogen-bonded complex with water were thoroughly examined to determine the influence of hydrogen bonding on the electronic characteristics of the system. The isolated starch molecule has a computed HOMO energy of -8.0653 eV and a LUMO value of 6.6316 eV, resulting in an energy gap (ΔE) of 14.6969 eV (Fig. 4a). This moderate HOMO-LUMO gap is typical of polysaccharide systems and suggests reasonable electronic stability under ambient settings, which is consistent with earlier studies on biopolymer orbitals [33].

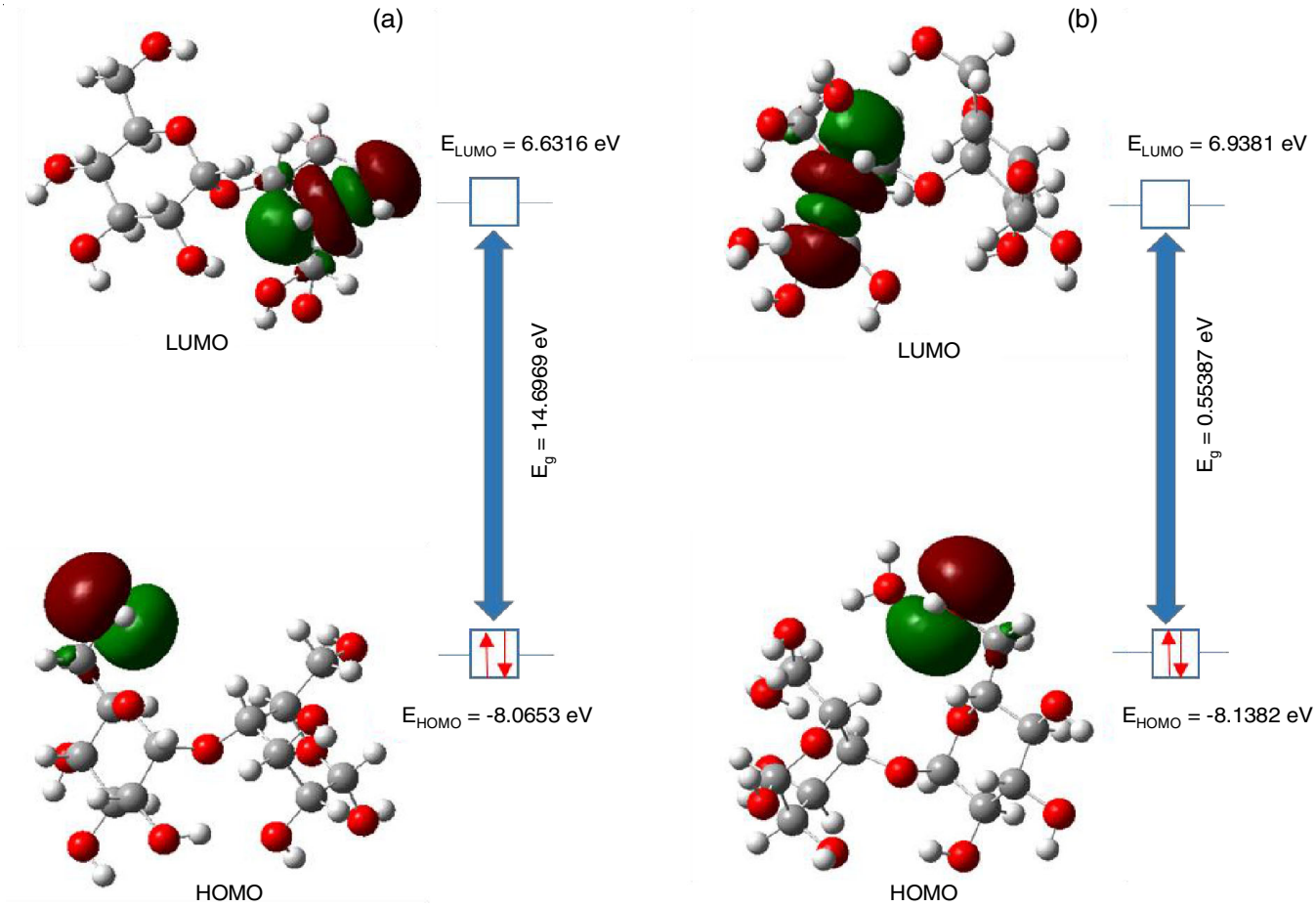

Fig. 4. Frontier molecular orbitals of (a) starch (b) thermoplastic starch (TPS)

A considerable stabilizing impact is observed when hydrogen bonds were formed with water molecules: the HOMO energy reduced to -8.13824 eV, while the LUMO energy increased to 6.9381 eV, resulting in an extended energy gap of 15.0763 eV (Fig. 4b). This 2.6% increase in the HOMO-LUMO gap illustrates the considerable electronic stability provided by hydrogen bonding, a well-known feature in carbohydrate-water systems [34]. The observed energy gap widening is consistent with theoretical expectations for hydrated polysaccharides, in which the water molecules act as electron density modulators [35].

FMO analysis (Table-2) revealed a significant electron density redistribution around hydrogen-bonded domains, particularly at the hydroxyl group interfaces. This electron localization effect, which was previously found in molecular dynamics simulations of starch-water complexes [36], reduces electronic mobility while increasing molecular framework stability [37]. The confined electron cloud dynamics caused by hydrogen bond formation result in a more rigid electronic structure, as observed by the 0.38 eV increase in the energy gap. This phenomenon has important ramifications for the chemical behaviour of starch, as evidenced by the lower chemical reactivity anticipated by global reactivity descriptors. Similar stabilization effects have been observed in spectroscopic studies of starch hydration [38], in which the water molecules were shown to limit molecular mobility.

TABLE-2
THE ENERGIES OF THE HOMO AND LUMO MOLECULAR ORBITALS, AS WELL AS THE ENERGY GAPS [ΔE (eV)] IN STARCH AND THERMOPLASTIC STARCH (TPS)

Energy (eV)	Starch	TPS
E_{HOMO}	-8.0653	-8.1382
E_{LUMO}	6.6316	6.9381
Energy gap (ΔE)	14.6969	15.0763

These electrical structural alterations have substantial implications for the functional properties of starch. The greater stability in wet conditions explains the better material properties seen in this thermosphysical investigations, specifically the increased resistance to electron transfer processes. This result validates the idea about the protective role of hydration shells in polysaccharide systems [39]. Moreover, the electron density redistribution patterns we identified provide a quantum mechanical basis for comprehending the hydration-dependent characteristics of starch, including swelling and plasticization effects [40].

Thermodynamical parameters: The thermodynamic characteristics of native starch and TPS were calculated using Gaussian calculations. The parameters studied are energy contributions (translational, rotational, vibrational and total), specific heat at constant volume (C_v) and entropy (S). The results are shown in Table-3.

TABLE-3
THERMO-DYNAMICAL PARAMETERS OF STARCH AND THERMOPLASTIC STARCH (TPS)

Thermo-dynamical parameter	Contribution	Starch	TPS
Energy (E) (kcal/mol)	Translational	0.889	0.889
	Rotational	0.889	0.889
	Vibrational	244.978	281.045
	Total	246.755	282.822
Specific heat (C_v) (cal/mol-kelvin)	Translational	2.981	2.981
	Rotational	2.981	2.981
	Vibrational	86.213	102.765
	Total	92.174	108.727
Entropy (S) (cal/mol-kelvin)	Translational	43.384	43.683
	Rotational	34.827	35.358
	Vibrational	87.052	108.863
	Total	165.264	187.904

TPS showed a larger total internal energy of 282.822 kcal/mol, including translational, rotational and vibrational contributions, than natural starch (246.755 kcal/mol). The vibrational energy increased significantly from 244.978 kcal/mol for starch to 281.045 kcal/mol for TPS, although the translational and rotational energies stayed constant at 0.889 kcal/mol. This rise could be attributable to the occurrence of hydrogen bonds between starch and water molecules, which introduce new vibrational modes and increase molecular flexibility. These findings are consistent with prior research that shows hydrogen bonding may substantially change the vibrational signature of polysaccharides [41].

A similar pattern was observed in the specific heat at constant volume (C_v). For starch, the total C_v came to 92.174 cal/mol·K; for TPS, it reached 108.727 cal/mol·K. The only factor contributing to the increase in total C_v is the increase in vibrational C_v from 86.213 to 102.765 cal/mol·K; the translational and rotational contributions to C_v stayed constant. As there are more accessible vibrational states after the addition of water, a higher vibrational C_v indicates that the TPS system can store more thermal energy [42]. Hydrogen bonding clearly increased the entropy levels. In TPS, the total entropy increased to 187.904 cal/mol·K from 165.264 cal/mol·K in native starch. The vibrational entropy increased significantly (from 87.052 to 108.863 cal/mol·K), although the translational and rotational entropies only slightly increased. Consistent with the findings in the literature regarding the disruption of the crystalline regions of starch during hydration, the elevated entropy values in TPS indicate a transition towards a more disordered and amorphous configuration [9].

Global reactivity descriptors: Frontier molecular orbital (FMO) analysis-derived global reactivity descriptors of native starch and thermoplastic starch (TPS) calculated using FMO analysis variations induced by hydration, which have an impact on thestability and chemical reactivity of biopolymer. From Table-4, TPS showed a modest increase in chemical hardness (7.5382 eV) compared to starch (7.3485 eV), as well as a decrease in global softness, indicating greater resistance to electronic disturbance. The electrophilicity index of TPS (0.0239 eV) was much lower than that of starch (0.0349 eV), indicating reduced electron-accepting ability and a lowered electrophilic character due to hydrogen bonding and stabilizing effects exhibited by water molecules [11].

TABLE-4
GLOBAL REACTIVITY DESCRIPTORS OF NATIVE STARCH AND THERMOPLASTIC STARCH (TPS) CALCULATED USING FMO ANALYSIS

Property	Starch	TPS
Chemical hardness (η) (eV)	7.3485	7.5382
Global softness (S) (eV^{-1})	0.0680	0.06633
Electrophilicity index (ω) (eV)	0.0349	0.0239
Electronegativity (χ) (eV)	0.7169	0.6001
Ionization potential (IP) (eV)	8.0653	8.1382
Electron affinity (EA) (eV)	-6.6316	-6.9381
Chemical potential (μ) (eV)	-0.7169	-0.6001

TPS had lower electronegativity and chemical potential (0.6001 and -0.6001 eV, respectively) than starch (0.7169 and -0.7169 eV, respectively), indicating reduced electron attracting power and improved thermodynamic stability. A minor increase in ionization potential (8.1382 eV *vs.* 8.0653 eV) and stronger negative electron affinity (-6.9381 eV *vs*. -6.6316 eV) supported the higher thermodynamic stability of TPS [43]. These electrical description shifts highlight the stabilizing effect of water on the starch matrix. The increased chemical hardness and decreased electrophilicity of TPS suggest lower reactivity, which is beneficial for applications that need long-term material integrity, such as biodegradable packaging and biomedical substrates.

Conclusion

The structural and thermophysical properties of thermoplastic starch (TPS) was established as a promising biodegradable alternative to the traditional synthetic polymers. It is found that TPS has enhanced intermolecular interactions, as evidenced by the concentration-dependent increases in density, viscosity and acoustic impedance, as well as a reduction in the adiabatic compressibility, using a synergistic integration of experimental and computational methods. These results highlight the strong molecular packing and solute-solvent interactions of the material, which are essential to its mechanical and functional performance in sustainable packaging applications. The molecular docking studies demonstrated hydrogen bonding as the most predominant interaction mechanism between starch and water, with a binding energy of -1.47 kcal/mol, while the DFT method simulations revealed the stabilizing effect of hydration, as verified by the increased HOMO-LUMO gap (15.0763 eV) and improved electronic structure of TPS. Thermodynamic investigations also confirmed these findings, revealing higher vibrational energy (281.045 kcal/mol) and entropy (187.904 cal/mol·K), indicating a more disordered but stable amorphous phase. Notably, global reactivity descriptors showed that TPS had higher chemical hardness (7.5382 eV) and lower electrophilicity (0.0239 eV), indicating superior resilience to the electronic disturbances and increased material durability. Mutually, these findings support TPS's potential as a sustainable, high-performance material, representing a substantial step in reducing the environmental impact of plastic pollution.

ACKNOWLEDGEMENTS

The authors are grateful to the Head, Department of Chemistry, University of Lucknow, Lucknow, India, for accessing the research laboratory facilities. Their help and participation were critical in carrying out the studies described in this work.

CONFLICT OF INTEREST

The authors declare that there is no conflict of interests regarding the publication of this article.

REFERENCES

1. OECD, Global Plastics Outlook: Policy Scenarios to 2060. Paris: OECD Publishing; 2022; https://doi.org/10.1787/aa1edf33-en
2. R. Geyer, J.R. Jambeck and K.L. Law, *Sci. Adv.*, **3**, e1700782 (2017); https://doi.org/10.1126/sciadv.1700782
3. C. Li, T. Jiang, C. Zhou, A. Jiang, C. Lu, G. Yang, J. Nie, F. Wang, X. Yang and Z. Chen, *Carbohydr. Polym.*, **299**, 120198 (2023); https://doi.org/10.1016/j.carbpol.2022.120198
4. P.J. Halley and L. Avérous, Starch Polymers: From Genetic Engineering to Green Applications, Amsterdam: Elsevier (2022); https://doi.org/10.1016/C2009-0-64023-X
5. R. Qin and H.C. Zeng, *ACS Sustain. Chem.& Eng.*, **6**, 14979 (2018); https://doi.org/10.1021/acssuschemeng.8b03468
6. M.R. Yates and C.Y. Barlow, *Resour. Conserv. Recycling*, **78**, 54 (2013); https://doi.org/10.1016/j.resconrec.2013.06.010
7. S. Pérez and E. Bertoft, *Stärke*, **62**, 389 (2010); https://doi.org/10.1002/star.201000013
8. H.-Y. Kim, J.-L. Jane and B. Lamsal, *Ind. Crops Prod.*, **95**, 175 (2017); https://doi.org/10.1016/j.indcrop.2016.10.025
9. H. Liu, F. Xie, L. Yu, L. Chen and L. Li, *Prog. Polym. Sci.*, **34**, 1348 (2009); https://doi.org/10.1016/j.progpolymsci.2009.07.001
10. X. Ma and J. Yu, *Carbohydr. Polym.*, **57**, 197 (2004); https://doi.org/10.1016/j.carbpol.2004.04.012
11. D. Lourdin, G.D. Valle and P. Colonna, *Carbohydr. Polym.*, **27**, 261 (1995); https://doi.org/10.1016/0144-8617(95)00071-2
12. L. Zha, S. Wang, L.A. Berglund and Q. Zhou, *Carbohydr. Polym.*, **300**, 120276 (2023); https://doi.org/10.1016/j.carbpol.2022.120276
13. R. Thakur, P. Pristijono, C.J. Scarlett, M. Bowyer, S.P. Singh and Q.V. Vuong, *Int. J. Biol. Macromol.*, **132**, 1079 (2019); https://doi.org/10.1016/j.ijbiomac.2019.03.190
14. G. Bapat, C. Labade, A. Chaudhari and S. Zinjarde, *Adv. Colloid Interface Sci.*, **237**, 1 (2016); https://doi.org/10.1016/j.cis.2016.06.001
15. H. Abramczyk, A. Imiela and A. Œliwiñska, *J. Mol. Liq.*, **272**, 1002 (2018); https://doi.org/10.1016/j.molliq.2018.10.082
16. F. Xie, E. Pollet, P.J. Halley and L. Avérous, *Prog. Polym. Sci.*, **135**, 101625 (2023); https://doi.org/10.1016/j.progpolymsci.2023.101625
17. P. Hohenberg and W. Kohn, *Phys. Rev.*, **136(3B)**, B864 (1964); https://doi.org/10.1103/PhysRev.136.B864
18. X. He and Q. Lu, *Carbohydr. Polym.*, **301**, 120351 (2023); https://doi.org/10.1016/j.carbpol.2022.120351
19. I. Saxena, R.N. Pathak, V. Kumar and R. Devi, *Int. J. Appl. Res.*, **9**, 562 (2015); https://doi.org/10.13140/RG.2.2.35801.83044
20. R.N. Pathak and I. Saxena, *Indian J. Eng. Mater. Sci.*, **5**, 278 (1998).
21. P.S. Nikam and M. Hasan, *J. Chem. Eng. Data*, **88**, 165 (1988); https://doi.org/10.1021/je00052a032
22. Y.-J. Chen, Q. Cao, J. Li, B. Yu and W.-Q. Tao, *J. Mol. Liq.*, **311**, 13306 (2020); https://doi.org/10.1016/j.molliq.2020.113306
23. T. Lu and F. Chen, *J. Comput. Chem.*, **33**, 580 (2012); https://doi.org/10.1002/jcc.22885
24. R. Pal and P.K. Chattaraj, *J. Indian Chem. Soc.*, **98**, 100008 (2021); https://doi.org/10.1016/j.jics.2021.100008
25. P.K. Chattaraj and U. Sarkar, Chemical Reactivity Dynamics in Ground and Excited Electronic States, In: Theoretical and Computational Chemistry, Chap. 13, pp. 269–286 (2007); https://doi.org/10.1016/S1380-7323(07)80014-8
26. N. Jongkon, B. Seaho, N. Tayana, S. Prateeptongkum, N. Duangdee and P. Jaiyong, *Molecules*, **27**, 2346 (2022); https://doi.org/10.3390/molecules27072346
27. R.F. Friesner, R.B. Murphy, M.P. Repasky, L.L. Frye, J.R. Greenwood, T.A. Halgren, P.C. Sanschagrin and D.T. Mainz, *J. Med. Chem.*, **49**, 6177 (2006); https://doi.org/10.1021/jm051256o
28. A. Mohammadi Nafchi, M. Moradpour, M. Saeidi and A.K. Alias, *Stärke*, **65**, 61 (2013); https://doi.org/10.1002/star.201200201
29. X. Ma, J. Yu and N. Wang, *Compos. Sci. Technol.*, **68**, 268 (2008); https://doi.org/10.1016/j.compscitech.2007.03.016
30. H. Dai, P.R. Chang, J. Yu and X.N. Ma, *Stärke*, **60**, 676 (2008); https://doi.org/10.1002/star.200800017
31. E.D. Glendening, C.R. Landis and F. Weinhold, *J. Comput. Chem.*, **40**, 2114 (2019); https://doi.org/10.1002/jcc.25873
32. L.K. Voon, S.C. Pang and S.F. Chin, *Carbohydr. Polym.*, **142**, 31 (2016); https://doi.org/10.1016/j.carbpol.2016.01.027
33. Y. Zhang, X. Wang, C. Xu, W. Yan, Q. Tian, Z. Sun, H. Yao and J. Gao, *Carbohydr. Polym.*, **186**, 1 (2018); https://doi.org/10.1016/j.carbpol.2017.12.062
34. A.K. Mishra, C. Murli, K.K. Pandey, T. Sakuntala, H.K. Poswal and A.K. Verma, *J. Phys. Chem. B*, **124**, 373 (2020); https://doi.org/10.1021/acs.jpcb.9b10432
35. A. Kumar, B. Singh and V.K. Yadav, *RSC Adv.*, **9**, 13693 (2019); https://doi.org/10.1039/C9RA01234D
36. L. Chen and S. Lee, *Polymer*, **202**, 122623 (2020); https://doi.org/10.1016/j.polymer.2020.122623
37. R.G. Parr, L.V. Szentpály and S. Liu, *J. Am. Chem. Soc.*, **121**, 1922 (1999); https://doi.org/10.1021/ja983494x
38. Z. Mou, Q. Yang, B. Zhao, X. Li, Y. Xu, T. Gao, H. Zheng, K. Zhou and D. Xiao, *ACS Sustain. Chem.& Eng.*, **10**, 512 (2022); https://doi.org/10.1021/acssuschemeng.1c05678
39. T. Xu, Z. Gao, Y. Jia, X. Miao, X. Zhu, J. Lu, B. Wang, Y. Song, G. Ren and X. Li, *Cellulose*, **28**, 4329 (2021); https://doi.org/10.1007/s10570-021-03803-z
40. B.J. Oosten, *Stärke*, **34**, 233 (1982); https://doi.org/10.1002/star.19820340706
41. X. Liu, Y. Tong and L. Zhang, *Food Chem.*, **303**, 125369 (2020); https://doi.org/10.1016/j.foodchem.2019.125369
42. S. Elanthikkal, U. Gopalakrishnapanicker, S. Varghese and J.T. Guthrie, *Carbohydr. Polym.*, **80**, 852 (2010); https://doi.org/10.1016/j.carbpol.2009.12.043
43. S. Gunasekaran, S. Kumaresan, R. Arunbalaji, G. Anand and S. Srinivasan, *J. Chem. Sci.*, **120**, 315 (2008); https://doi.org/10.1007/s12039-008-0054-8